

### Simulations reveal the role of composition into the atomic-level flexibility of bioactive glass cements

Kun Viviana Tian, Gregory A. Chass\* and Devis Di Tommaso\*

Bioactive glass ionomer cements (GICs), the reaction product of a fluoro-alumino-silicate glass and poly-acrylic acid, have been in effective use in dentistry for over 40 years and more recently in orthopaedics and medical implantation.

Q1 Q2

Q5

Please check this proof carefully. **Our staff will not read it in detail after you have returned it.**

Translation errors between word-processor files and typesetting systems can occur so the whole proof needs to be read. Please pay particular attention to: tabulated material; equations; numerical data; figures and graphics; and references. If you have not already indicated the corresponding author(s) please mark their name(s) with an asterisk. Please e-mail a list of corrections or the PDF with electronic notes attached – do not change the text within the PDF file or send a revised manuscript. Corrections at this stage should be minor and not involve extensive changes. All corrections must be sent at the same time.

**Please bear in mind that minor layout improvements, e.g. in line breaking, table widths and graphic placement, are routinely applied to the final version.**

Please note that, in the typefaces we use, an italic vee looks like this:  $\nu$ , and a Greek nu looks like this:  $\nu$ .

We will publish articles on the web as soon as possible after receiving your corrections; **no late corrections will be made.**

Please return your **final** corrections, where possible within **48 hours** of receipt, by e-mail to: pccp@rsc.org

## Queries for the attention of the authors



Journal: PCCP

Paper: c5cp05650k

Title: **Simulations reveal the role of composition into the atomic-level flexibility of bioactive glass cements**

Editor's queries are marked on your proof like this , , etc. and for your convenience line numbers are indicated like this 5, 10, 15, ...

Please ensure that all queries are answered when returning your proof corrections so that publication of your article is not delayed.

Query reference	Query	Remarks
Q1	For your information: You can cite this article before you receive notification of the page numbers by using the following format: (authors), Phys. Chem. Chem. Phys., (year), DOI: 10.1039/c5cp05650k.	OK
Q2	Please carefully check the spelling of all author names. This is important for the correct indexing and future citation of your article. No late corrections can be made.	Checked
Q3	Do you wish to add an e-mail address for the corresponding author? If so, please supply the e-mail address.	Gregory A. Chass: g.chass@qmul.ac.uk Devis Di Tommaso: d.ditommaso@qmul.ac.uk
Q4	Address b appears to be incomplete. Do you wish to provide any further details? If so, please provide the details.	Yes, it is "Global Institute of Computational Molecular and Materials Science (GIOCOMMS), Budapest/Beijing/Toronto"
Q5	Please check that the inserted Graphical Abstract image and text are suitable. Please ensure that the text fits between the two horizontal lines.	The text needs to be revised. See corrections on the first page.
Q6	As the equations appeared to be labelled out of numerical order, the equations have been renumbered. Please check that the renumbering is correct and that all of the citations within the text correspond to the correct equation, and indicate any changes required.	The equations have been correctly renumbered.
Q7	Ref. 12: Please provide the initial(s) for the 2nd author.	Ref 12. L. Forsten, Scand. J. Dent. Res., 1977, 85, 503–504.
Q8	Ref. 40: Can this reference be updated?	
Q9	Please indicate where ref. 78 should be cited in the text.	

# 10 Simulations reveal the role of composition into the atomic-level flexibility of bioactive glass cements†

15 Kun Viviana Tian,<sup>ab</sup> Gregory A. Chass<sup>\*ab</sup> and Devis Di Tommaso<sup>\*c</sup>

20 Bioactive glass ionomer cements (GICs), the reaction product of a fluoro–alumino–silicate glass and poly-acrylic acid, have been in effective use in dentistry for over 40 years and more recently in orthopaedics and medical implantation. Their desirable properties have affirmed GIC's place in the medical materials community, yet are limited to non-load bearing applications due to the brittle nature of the hardened composite cement, thought to arise from the glass component and the interfaces it forms. Towards helping resolve the fundamental bases of the mechanical shortcomings of GICs, we report the 1st ever computational models of a GIC-relevant component. *Ab initio* molecular dynamics simulations were employed to generate and characterise three fluoro–alumino–silicate glasses of differing compositions with focus on resolving the atomic scale structural and dynamic contributions of aluminium, phosphorous and fluorine. Analyses of the glasses revealed rising F-content affecting an expansion of the glass network, compression of Al–F bonding, angular constraint at Al-pivots, localisation of alumino–phosphates and increased fluorine diffusion. Together, these changes to the structure, speciation and dynamics with raised fluorine content impart an overall rigidifying effect on the glass network, and suggest a predisposition to atomic-level inflexibility, which could manifest in the ionomer cements they form.

25 Received 21st September 2015,  
Accepted 12th November 2015

DOI: 10.1039/c5cp05650k

30 www.rsc.org/pccp

## 35 Introduction

35 Bioactive glasses and related glass cements have drawn attention for their potential use as synthetic bone graft substitutes as well as in the repair and replacement of damaged bones and teeth.<sup>1,2</sup> Glass ionomer (or polyalkenoate) cements (GICs), have been successfully used in dentistry as luting cements and anterior restorative materials since their introduction in the early 1970s by the British Technology Group<sup>3,4</sup> – and remain their 2nd biggest earner for chemical technology. As a mercury (Hg) free alternative to dental amalgams these glass–polymer composites are specifically highlighted in the EU commission report: Study on the Potential for Reducing Mercury Pollution from Dental Amalgam and Batteries, as being “cost-effective and environmentally-friendly Hg-free restoration”.<sup>5</sup> With strict regulations and actions recently coming into effect (1st January, 2014) short- and long-term future growth is assured,

35 particularly in combination with the rapid developments in bone-remineralisation and hydroxyapatite-coated implantation.<sup>6</sup> This is further buoyed by GICs being ideally suited for and extensively used in atraumatic restorative treatment (ART), in developing nations in particular, with tooth fillings being prepared and completed without requirement of electric instruments or anesthetic.<sup>7–9</sup>

40 The pervasive use of GICs is due to the following desirable properties: good biocompatibility,<sup>10,11</sup> tooth-like colour and appearance, antibacterial and anticariogenic properties *via* lasting fluoride release,<sup>12–15</sup> minimised interfacial leakage, attributable to low setting shrinkage, a thermal expansion coefficient similar to that of tooth,<sup>16</sup> and direct durable bonding to tooth and bone<sup>17</sup> through development of a dynamic interfacial “ion-exchange” layer containing ions both from the tooth and the GICs.<sup>18,19</sup>

50 With some of these properties transferable to other fields of medicine, for example, successful applications in various otorhinolaryngological and maxillofacial reconstructive surgeries and augmentation,<sup>20–22</sup> much attention was focused on developing an *in situ* setting glass ionomer bone cement in the 1990s.<sup>23</sup> The initial positive *in vivo* biocompatibility and bone tissue responses have confirmed their osteoconduction and osteointegration.<sup>23–25</sup> Studies have found GICs to be bioactive in the bone environment

<sup>a</sup> Materials Science Research Institute, Department of Oral Diagnostics,

<sup>b</sup> Faculty of Dentistry, Semmelweis University, Budapest 1088, Hungary

<sup>c</sup> Global Institute of Computational Molecular and Materials Science (GI-COMMS),

<sup>d</sup> School of Biological and Chemical Sciences, Queen Mary University of London,

Mile End Road, London, E1 4NS, UK

† Electronic supplementary information (ESI) available. See DOI: 10.1039/c5cp05650k

1 *via* the persistent release of  $\text{Ca}^{2+}$ ,  $\text{PO}_4^{3-}$  and  $\text{F}^-$  ions. As with  
 2 bioglasses, a siliceous hydrogel ( $\text{Si}(\text{OH})_4 \cdot n\text{H}_2\text{O}$ ) forms on the  
 3 glass surface from degradation and raising homogeneity – overall  
 4 beneficial to biocompatibility.<sup>23</sup>

5 Although clinical evaluations of GI bone cements have  
 6 reported few extreme cases of adverse effects,<sup>26,27</sup> there is  
 7 evidence suggesting that good surgical technique and applica-  
 8 tions outside the restricted area can further reduce their  
 9 diminutive toxicity.<sup>23</sup>

10 GICs are therefore near ideal dental, implant and osteo-  
 11 restorative materials, yet, similar to bioactive glasses, GICs  
 12 are brittle and currently only applicable to intermediate load-  
 13 bearing applications.<sup>28</sup> Extensive efforts have been undertaken  
 14 to improve the damage tolerance of GICs, principally *via*  
 15 reinforcement of the filler (unreacted glass) in addition to  
 16 modification of the constituent components towards perfor-  
 17 mance improvement.<sup>29,30</sup> However, mechanical amendment  
 18 has been incremental, due to lack of understanding of the  
 19 atomic structure and setting mechanism.<sup>31</sup>

20 GIC composite cement is formed *via* acid–base reactions  
 21 between a polyalkenoic acid, such as polyacrylic acid (PAA)  
 22 [ $\text{CH}_2-\text{CH}(\text{COOH})_n-\text{CH}_3$ ,  $n \approx 319$ ],<sup>3,4</sup> and/or its copoly-  
 23 mers of acrylic-itaconic, maleic, methacrylic acids, and the  
 24 alkaline ion leachable fluoro–alumino–silicate glass powder  
 25 ( $\text{SiO}_2-\text{Al}_2\text{O}_3-\text{CaF}_2$ ).<sup>32</sup> Their general structure involves unreacted  
 26 glass particles (filler) tethered within a matrix of salt hydro-  
 27 gels formed by the metal ions leached from the glass cross-linking  
 28 the polyalkenoic acid (Fig. 1).<sup>42</sup> The glass component is  
 29 known as an ionomer glass, with compositions similar to the  
 30 fluoride-containing bioglass developed by Hench *et al.*<sup>33</sup>  
 31 All GICs employ the same complex ion leachable glass pro-  
 32 duced through a melt–shock–cool routine.<sup>34</sup> The glasses

are characteristics of high  $\text{Al}_2\text{O}_3:\text{SiO}_2$  mass ratios  $\geq 0.5$  and  
 elevated fluorine content.<sup>35</sup>

Studies have shown that the composition of the ionomer  
 glass has a profound influence on the properties of the dental  
 cement,<sup>36,37</sup> and empirical rules have been proposed regard-  
 ing the structural role of each atom in the glass during the setting  
 reaction and on the cement properties.<sup>38</sup> The atomic structure  
 of ionomer glasses therefore remains poorly understood.

We therefore initiated state-of-art quantum chemical mod-  
 elling to resolve the influence of atomic composition on the  
 nano-scale structural and dynamical properties of the ionomer  
 glass. Focus was on the local atomic structure and dynamics  
 (Al-centres have been evidenced as being primarily responsible  
 for the formation of the interface),<sup>39,40</sup> as well as fluoride  
 diffusion, towards resolving any predisposition in the glass  
 component to manifest the practical and clinical properties of  
 GICs; its lacking flexibility in particular.

## Materials and methods

### Glass compositions

Commercial G338 glass ( $\text{Si}_{21}\text{Al}_{34}\text{Ca}_9\text{Na}_{17}\text{F}_{56}\text{P}_{11}\text{O}_{110}$ ), a 6-  
 component, 7-element glass and the basis of most commercial  
 GICs, with high fluorite and phosphate content, was chosen for  
 this work. Two additional fluoro–alumino–silicate glasses with  
 similar  $\text{Al}_2\text{O}_3:\text{SiO}_2$  and Al:Si + P ratios as those in G338 were  
 also characterised. Specifically, a fundamental 3-component,  
 5-element (G3) cement-forming glass ( $\text{Si}_{26}\text{Al}_{18}\text{Ca}_{10}\text{F}_{20}\text{O}_{79}$ ) and  
 its phosphate augmented 4-component, 6-element (G4) analo-  
 gue ( $\text{Si}_{18}\text{Al}_{26}\text{Ca}_{15}\text{F}_{30}\text{P}_{10}\text{O}_{100}$ ). These three related models  
 allowed for comparative analyses of the influence of introduc-  
 ing phosphate and sodium, as well as raised fluorine content  
 (13% in G3, 15% in G4 and 22% in G338) on the structure and  
 dynamics of the glass. The real chemical systems were mod-  
 elled, ensuring evolved sampling from multiple chelation cen-  
 tres, avoiding limitations of associated with ambiguous cation  
 chelations.<sup>41</sup> Relative atomic compositions and unit cell sizes  
 of these glass models are listed in Table 1 (see also ESI,†  
 Section S1).

### Simulation details

**Overview of modelling.** We employed *ab initio* (Born–Oppen-  
 heimer) molecular dynamics (AIMD) simulations, using the  
 electronic structure code CP2K/Quickstep code, version  
 2.6.<sup>42,43</sup> This parameter-free, first principle approach repre-  
 sents the most physically accurate means to introducing polar-  
 ization and other fundamental electronic effects in the MD  
 model – supporting a much wider applicability than classical

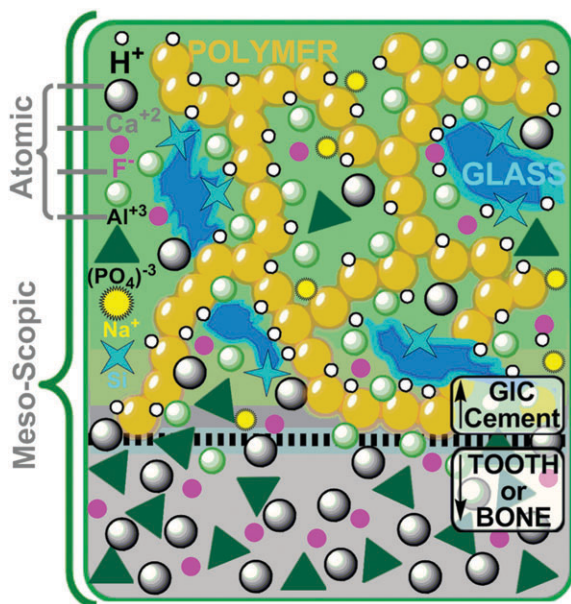


Fig. 1 Qualitative representation of the atomic through meso-scopic  
 structure of a GIC composite forming an ion-exchange interface with  
 hydroxyapatite in tooth or bone.

Table 1 Relative compositions (mol%) and unit cell size (Å) in the three  
 ionomer glass models characterised in this work

Model	$\text{SiO}_2$	$\text{Al}_2\text{O}_3$	$\text{CaF}_2$	$\text{AlPO}_4$	$\text{AlF}_3$	$\text{NaF}$	Cell size (Å)
G3	57.8	20.0	22.2	—	—	—	13.1153
G4	35.3	15.7	29.4	19.6	—	—	14.3690
G338	28.8	11.0	12.3	15.1	9.6	23.3	15.5393

MD.<sup>44,45</sup> AIMD explicitly imposes an electronic structure and quantum chemical based energetic potentials that is representative of the real physical systems. The methodological rigorosity makes AIMD an ideal tool to investigate the structural and dynamical properties of complex, multicomponent glasses, and this technique is thus very useful in complementing and supporting experiments towards a fundamental understanding of the properties of amorphous materials.<sup>46</sup>

**Computational methods.** CP2K implements density functional theory (DFT) based on a hybrid Gaussian plane wave (GPW) approach.<sup>47</sup> The Perdew–Burke–Ernzerhof (PBE) density functional was used for the exchange correlation.<sup>48</sup> Previous studies have shown PBE makes accurate predictions of the structural, dynamical and electronic properties of phosphate,<sup>49</sup> phospho-silicate,<sup>50</sup> and alumino-silicate glasses.<sup>51</sup> Goedecker–Teter–Hutter pseudopotentials<sup>52</sup> were employed to avoid resource-intensive determinations of core configurations. All atomic species were represented using a double-zeta valence polarized basis set. The plane wave kinetic energy cut off was set to 1000 Ry. Simulations were carried out with a wave function optimization tolerance of  $10^{-6}$  au that allows for 1.0 fs time steps with reasonable energy conservation. Periodic boundary conditions were used throughout.

**Simulation protocol.** The structures of the G3, G4 and G338 glasses were generated using a full AIMD melt-and-quench procedure (Scheme 1).

In order to generate an unbiased initial geometry, constituent atoms for each model were randomly placed in a cubic periodic box (unit cell) and subjected to the inter-atomic constraints as follows: Y–T pairs  $\geq 1.65$  Å (Y = Si, Al, P, and T = O, F); M–T pairs  $\geq 2.10$  Å (M = Ca, Na); all other atomic-pairs  $\geq 2.60$  Å. Unit cell size was fixed to the empirically-observed density of ionomer glasses ( $2.4 \pm 0.3$  g cm<sup>-3</sup>).<sup>40,53</sup> The initial structure was subject to 40 steps of geometry optimisation, using the conjugate gradient algorithm, to relax strain imposed from randomisation. The resultant configurations were then subjected to a simulated annealing process, wherein the structures were allowed to relax in the *NVE* (constant number of particles (*N*), volume (*V*) and energy (*E*)) ensemble for 10 ps. This was followed by a series of *NVT* (constant number of particles, volume and temperature) runs of approximately 20 ps each, whose target temperatures were set at 300 K intervals from 3000 K down to 600 K. Finally, at 300 K the glasses were allowed to equilibrate (production phase) for 100 ps, generating a room-temperature structure. This cooling phase, albeit much

quicker than empirical rates (currently impossible to achieve computationally), corresponds to a rate close to the value of 10 K ps<sup>-1</sup> suggested by Tilocca to obtain convergent local- and medium-range properties,<sup>54</sup> and faster than the cooling rates previously reported in the generation of phosphate, phospho-silicate, and alumino-silicate glasses using the full *ab initio* melt and quench approach.<sup>49,55–58</sup> As pointed out in a recent computational investigation, the structural and vibrational properties of alumina-silicate glasses prepared by a “full” AIMD calculation are significantly better, compared to the experimental one, than samples prepared by molecular dynamics simulations using empirical force fields.<sup>59</sup> With regard to the choice of ensemble, *NVT* simulations are computationally less demanding than the *NPT* ensemble when running *ab initio* MD simulations, whilst maintaining good agreement with experiment. In fact, for DFT plane wave MD simulations in the *NPT* ensemble the convergence of the pressure requires a significantly higher basis set cut-off than can be used for *NVT* FPMD simulations,<sup>60</sup> thereby leading to a substantial increase in computational time. Another problem, particularly for liquids, is that the equilibration time for *NPT* dynamics can be significantly larger.<sup>60</sup>

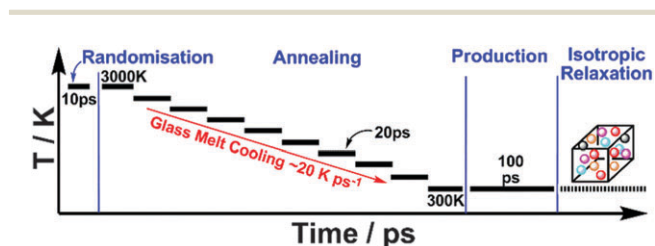
The last configuration of the MD trajectory at 300 K of the bulk glasses was then subject to isotropic relaxation of the volume of the cubic cell to obtain the optimal (theoretical) volume. For all glasses, the resultant optimised lattice parameters were within 0.8% of those giving rise to the experimental density, evidencing the bulk sample as being representative of the real glass systems (Fig. S2, ESI†). The theoretical densities of the glass ionomers were 2.34 g cm<sup>-3</sup> for G338 ( $\epsilon = -2.5\%$ ), 2.42 g cm<sup>-3</sup> ( $\epsilon = 0.8\%$ ) for G4, and 2.43 g cm<sup>-3</sup> ( $\epsilon = 1.3\%$ ) for G3.

## Results and discussion

Fig. 2 shows a snapshot from the AIMD trajectories at 300 K for each of the three equilibrated glasses. The most evident structural difference is the increased cross-link density within the network on going from the 3-component G3 glasses to the 6-component commercial G338 system. Overall, these glasses are comprised of Si–O–Si, Si–O–Al and Al–O–Al networks, which serve as the ‘building blocks’ for these glasses. Negative charges at AlO<sub>4</sub> and AlO<sub>x</sub>F<sub>4-x</sub> (where  $x = 1-4$ ) sites are charge-balanced by Ca<sup>2+</sup>/Na<sup>+</sup> ions. In systems also containing significant amount of phosphorus (G4 and G338), the PO<sub>4</sub> tetrahedra are also network formers and the negatively charged phosphates locally charge-balance the aluminium within the glass network. Any extraneous Ca<sup>2+</sup>/Na<sup>+</sup> ions act as network modifiers, fragmenting the glass network, raising the non-bridging oxygen (NBO) to bridging-oxygen (BO) ratio (NBO : BO) (Fig. 2).

### Network connectivity and Al-coordination

One of the main structural parameters to quantify the network fragmentation of glasses is the network connectivity (NC),



Scheme 1 Schematic depiction of the AIMD melt-quench simulation protocol employed to generate the unit cells of the glass models.

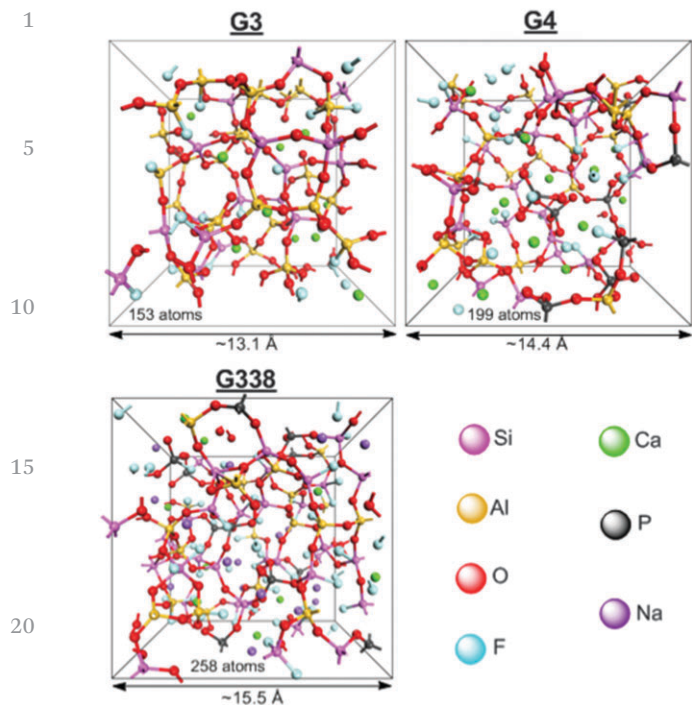


Fig. 2 Views of the annealed and isotropically-relaxed structures of the 3-(G3), 4-(G4) and 6-component (G338) glasses simulated in the present study; unit cell properties are included. Si–O–Si, Si–O–Al, Al–O–Al networks form the core structure of the glasses, with  $\text{Ca}^{2+}/\text{Na}^{+}$  ions and phosphates providing local-charge balance. Extraneous cations act as network modifiers, rupturing the glass network, raising NBO : BO ratios.

representative of the average number of BO atoms per glass forming species (Si, Al and P):<sup>61</sup>

$$\text{NC} = \sum_i p(Q^i) \times i \quad (1)$$

where  $p(Q^i) = Q^i / \sum Q^j$  and  $Q^n$  is the number of glass forming species with  $n$  BOs. For instance, the structure of pure silica glass consists of only  $Q^4$  species forming a three-dimensional network and  $\text{NC} = 4$ . On the other hand, low NCs denote open and fragmented glass structures.

Table 2 summarises the network connectivity and average coordination number of Al for the three glass compositions (full analysis of the  $Q^n$  distributions is in ESI† Table S3). The Al atom is on average surrounded by 4.2 atoms (oxygen and/or fluorine), which is very close to the average nearest neighbour numbers obtained for amorphous  $\text{Al}_2\text{O}_3$  by experiment (4.1)<sup>62</sup> and

Table 2 Network connectivity for network forming species (Si, Al, P), relative Al coordinations (%) and averages for the G3, G4 and G338 glasses. Standard error of the Al-coordinations computed from the variation of 10 block averages is  $\pm 0.002$ – $0.05\%$

	$\text{NC}_{\text{Si-O-X}}$	$\text{NC}_{\text{Al-O-X}}$	$\text{NC}_{\text{P-O-X}}$	$\text{Al}^{\text{IV}}$	$\text{Al}^{\text{V}}$	$\text{Al}^{\text{VI}}$	$\text{Al}^{\text{avg}}$
G3	3.52	3.83	—	83.6	16.4	0.0	4.16
G4	3.99	3.57	2.04	82.7	17.3	0.0	4.17
G338	3.40	3.37	2.65	80.3	18.1	1.6	4.21

X = Si, Al, P in Si–O–X, Al–O–X, P–O–X.

simulations (4.25).<sup>63,64</sup> Therefore, the majority of aluminium atoms maintain tetrahedral coordination in the three glasses, although a slight rise in Al-coordination (4.5  $\rightarrow$  6) is promoted by the additions of fluorine, phosphorus and sodium. It has been suggested that the increase of Al-coordination from (iv) to (vi) promotes the cross-linking of the  $\text{Al}$  in the cement matrix,<sup>31</sup> increases the strength (Young's modulus) and concomitantly reduces the toughness and plasticity of GICs.<sup>38,40</sup>

NMR results show that in G338 glass there is a predominance of  $\text{Al}^{\text{IV}}$  accompanied by a minority of  $\text{Al}^{\text{V}}$  and  $\text{Al}^{\text{VI}}$  species.<sup>65,66</sup> Lowenstein's two conditions for maintaining Al in a four-fold coordination state, require an  $\text{Al} : (\text{Si} + \text{P})$  ratio  $\leq 1.0$  and sufficient P and network-forming cations to balance the charge deficient  $\text{AlO}_4$  tetrahedron;<sup>67</sup> the presence of  $\text{Al}^{\text{V}}$  and  $\text{Al}^{\text{VI}}$  are therefore surprising. However, the higher coordination states have been linked with the formation of aluminofluorine species of the type  $[\text{AlO}_x\text{F}_y]^{n-}$ ; these species exist in our model glasses (listed in Table S4, ESI†). Trends show that the populations of  $\text{AlO}_x\text{F}_y$  species ( $1 \leq x, y \leq 3$ ) increases (51%  $\rightarrow$  77%  $\rightarrow$  80%) as fluorine content is increased, respectively for the G3  $\rightarrow$  G4  $\rightarrow$  G338 system succession (Table S4, ESI†), in agreement with related magic angle spinning nuclear magnetic resonance (MAS-NMR), which have revealed the formation of aluminium oxyfluoride.<sup>68</sup>

This marked progression to hetero-atomic bonding together with rising fluorine and phosphorous (G4) and subsequently sodium (G338) content, constrains the T–Al–T angular distribution from its wide angular distribution covering  $\sim 85$ – $135^\circ$  towards ideal tetrahedrality ( $109.5^\circ$ ), further evidencing the overall rigidifying effect of these ions.<sup>69</sup> These findings are in-line with proposals for Al possibly becoming over chelated and thus disadvantageously constrained, as is known in other materials.<sup>70</sup>

### Inter-atomic bonding

Inter-atomic bonding pairs were analysed through generation of radial distribution functions (RDF),  $g_{\alpha\beta}(r)$ . RDFs represent the probability, relative to a random distribution, of finding atoms of types  $\alpha$  and  $\beta$  separated by a distance  $r$ . RDFs for Si–O, Al–O, P–O, CaF and Ca–O show little change, Al–F and to a lesser extent Si–F show slight compression (Fig. 3 and Fig. S5, ESI†).

Of practical interest is Al-bonding, as Al-centres have been evidenced as being primarily responsible for the formation of the interfaces.<sup>31</sup> Fig. 3 displays the first peak of the RDFs of the Al–O and Al–F pairs obtained from the AIMD simulations. For all three glasses, the first peak in the Al–O RDF occurs at  $\sim 1.76$  Å, which is close to the values found in amorphous aluminium oxide ( $\text{Al}_2\text{O}_3$ ) using classical and *ab initio* MD simulations.<sup>62,63</sup> The position of the first peak for Al–F RDFs occurs at 1.76 Å in G3 and G4, reducing to 1.73 Å in G338. Albeit relatively small geometrically, the analysis of the standard errors of the mean of the Al–F RDFs (Fig. S6, ESI†) confirmed that the bond compression effected by raised fluorine, phosphorous and sodium content in the glass is not trivial. The higher content of F, P, and to a lesser extent Na, increases the

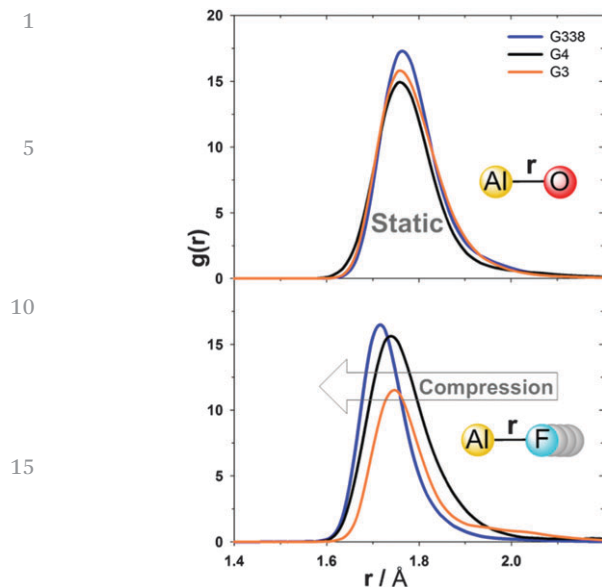


Fig. 3 Radial distribution functions over the 1.4–2.2 Å range for the Al–O (Top) and Al–F (Bottom) atomic-pairs in the G3, G4 and G338 glasses. Although Al–O bonding geometry remains relatively static, the Al–F pair shows slight compression with rising fluorine, phosphate and sodium content.

rigidity of the local coordination of Al in the glasses. This translates to a greater degree of stress in the G338 glass during melt-quenching production, relative to the other systems.<sup>71</sup>

### Structural pivots

Three-center atomic motifs were analysed through generation of angular distribution functions (ADFs),  $\rho(\theta)$ , for the network forming Si, Al and P atoms. ADFs for T–Si–T and T–P–T trios, where T = O or F, showed little change (Fig. S7, ESI†).

With respect to the interface-forming Al, T–Al–T bond-angle distributions showed pronounced change upon addition firstly of P and subsequently F (Fig. 4). The distribution for the

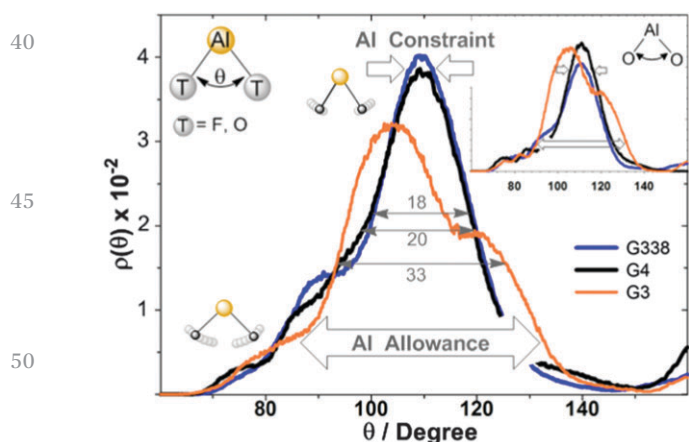


Fig. 4 The T–Al–T angular distribution function, T = O or F, for the G3, G4 G338 glasses; O–Al–O angular distribution functions are shown in the inset. Angular constraint at Al is observed in both T–Al–T and O–Al–O with rising F<sup>−</sup> and PO<sub>4</sub><sup>3−</sup> content.

fundamental G3 glass is relatively broad with respect to the other glasses, and shows two shoulders at ~105° and 120°. However, as the content of fluorine and phosphorous (G4) and subsequently sodium (G338) are increased in the glass, the T–Al–T distribution tapers to ideal tetrahedrality (109.5°) (Fig. 4). The full width at half maximum (FWHM) values of the T–Al–T ADFs quantify this angular constriction from 33° in G3 to 20° in G4 and 18° in G338.

Similar stiffening is observed for the O–Al–O bond-angle distributions (Fig. 4, inset), with FWHM narrowing from 30° in G3, to ~20° in G4 and G338. Higher content of F, P, and to a lesser extent Na, in the glass therefore increases angular rigidity of the local coordination of Al in the glasses.

Analysis of the standard errors of the mean of the ADFs (Fig. S8, ESI†) confirmed the near halving of the T–Al–T and O–Al–O angle flexibility with each successive increase in compositional complexity, resulting in constraint of local aluminium structure. This is in indirect agreement with empirically observed rise in F-content raising (compressive and tensile) strength and lowering toughness in related systems.<sup>34,38</sup>

### Al dynamics

Towards resolving the origin of the increased rigidity of local Al coordination, the velocity-autocorrelation function (VACF) of the aluminium atoms was computed. VACF is defined as follows:

$$\text{VACF}_{\text{Al}}(t) = \frac{1}{N_{\text{O}} N_{\text{Al}}} \sum_{j=1}^{N_{\text{O}}} \sum_{i=1}^{N_{\text{Al}}} v_i(t_j) \cdot v_i(t_j + t) \quad (2)$$

where  $v_i$  is the velocity vector of atom  $i$ ,  $N_{\text{O}}$  and  $N_{\text{Al}}$  are the number of time origins spaced by  $t$  and number of Al atoms, respectively. The VACFs of Al for the G3, G4 and G338 glasses are plotted in Fig. 5.

In general, the occurrence of a dip to negative values in the VACF profile results from the so-called “cage effect” for the tagged particle, that is, it takes some time for the particle to escape from the cage formed by its surrounding neighbours.<sup>72</sup>

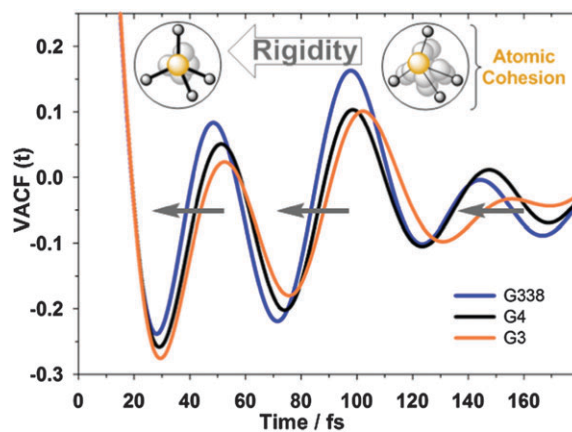


Fig. 5 The velocity autocorrelation function (VACF) of the Al atoms, showing the increase of rigidity of the local Al-coordination for the G3, G4 and G338 glasses.

The oscillatory behaviour and position of the first minimum ( $t_0$ ) of the VACF can then be used to probe the interaction of the tagged particle with the surrounding cage.<sup>73</sup> For example, rigid intra-molecular vibrations lead to a fast oscillatory trend for the VACFs of the network formers Si and P ( $t_0 = 0.02$  ps) (Fig. S9, ESI†) and to a lesser extent of Al ( $t_0 = 0.03$  ps) (Fig. 5). On the other hand, whereas the glass modifiers Ca and Na show a much broader first minimum ( $t_0 = 0.08$  ps for Ca and  $t_0 = 0.1$  ps FOR Na), which is not followed by a marked oscillatory behaviour as the interaction of these cations with the surrounding cage is weaker (Fig. S9, ESI†).

Therefore, changes in the profiles of the VACF of aluminium atoms (oscillatory behaviour and position of the first minimum) with the composition of the glasses are descriptors of the strength of Al-interaction with the surrounding atoms and of the rigidity of the intra-molecular vibration (Fig. 5). Compared with the fundamental  $\text{SiO}_2\text{-Al}_2\text{O}_3\text{-CaF}_2$  system (G3), the addition of F and P (G4) and subsequently Na (G338) into the glass leads to a more marked oscillatory behavior of the VACF (Fig. 5). This is indicative of the strengthening of Al-interaction with the surrounding 'cage' and a more rigid intra-tetrahedral vibration. This dynamic rigidity further highlights the constraint of Al to a definite and inflexible geometry upon increase of fluorine, phosphorus and sodium content.

### Phosphate networks

It has been proposed that the presence of phosphate in the glass induces the formation of Al-O-P bonds, reducing aluminium precipitation, resulting in  $\text{PO}_4^{3-}$  units competing with the carboxylic groups ( $\text{COO}^-$ ) on PAA for cations.<sup>37</sup> Increased phosphate content is evidenced as affecting an initial increase in compressive strength followed by a sharp reduction thereof, and thus may be a dominant contributor to long-term cement properties.<sup>74,75</sup> Experimental evidence of relevant Al-phosphate (Al-O-P) formation in related glasses<sup>68,76,77</sup> provides another important metric to track structural characteristics and was thus explored in this work. RDFs for the Al-P pair in the phosphate-containing glasses G4 and G338 are presented in Fig. 6.

Although Al and P would never be directly bonded, such distributions can reveal their contiguity and thus the tendency for Al-O-P and pyrophosphate (P-O-P) speciation in a given system.

In both systems the first peak occurs at  $\sim 3.1$  Å, which is lower than the sum of the Al-O (1.76 Å) and P-O (1.54 Å) bond lengths (Fig. 6), evidencing the formation of Al-O-P units in phosphate-containing glasses (G4 and G338 in this case).

Even with unrealistic Al-O-P bond angles of  $180^\circ$ , Al and P separated by  $3.30$  Å ( $1.76 + 1.54$  Å) or more would corroborate the absence of Al-O-P species. P-O-P groups are concluded as not developing from the P-P pair RDFs (Fig. 6). These show average phosphorous-phosphorous distances of  $\sim 3.9$  and  $4.3$  Å in G4 and G338, respectively, which are both significantly higher than twice the average P-O distance (1.54 Å).

As with silica gel formation in bioglasses, an analogous aluminophosphate gel ( $\text{AlPO}_x\text{F}_y$ , where  $x = 5-7$ ,  $y = 7 - x$ )

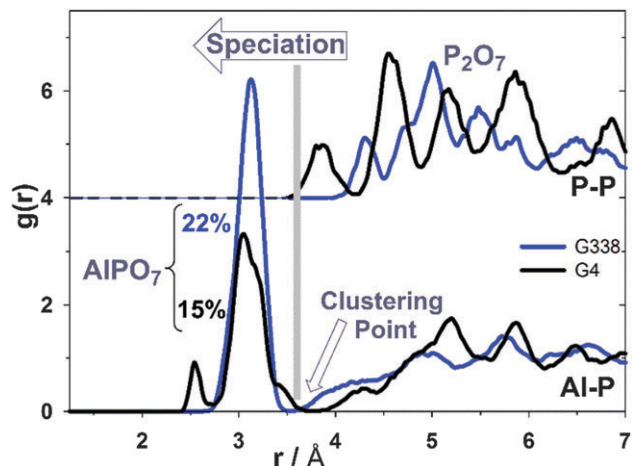


Fig. 6 The radial distribution function of the Al-P and P-P atom pairs obtained from the AIMD simulations of the G4 and G338 ionomer glasses. The clustering point below which localised phosphate-species form is indicated. For clarity, the baseline of the P-P radial distribution function has been shifted.

forms, in agreement with empirical observations.<sup>74-77</sup> This is exemplified by the non-zero  $g(r)$  values below the clustering point where speciation develops (Fig. 6). Increased F content raises the  $\text{AlPO}_x\text{F}_y$  content from 14.9% in G4 to 21.8% in G338 (Table S10, ESI†). The relatively low P-F coordination (5 and 6%, respectively in G4 and G338, Table S11, ESI†) indicates that the majority of these species are  $\text{AlPO}_7$ , with a minor fraction of  $\text{AlPO}_6\text{F}$  and  $\text{AlPO}_5\text{F}_2$ , with F predominantly bound to Al.

### Fluorine - environs and diffusion

The proportion of  $\text{FAlCa}$ ,  $\text{FAlNa}$ ,  $\text{FCa}$  and  $\text{FNa}$  species (where F is the central atom) increased with rising fluorine content concurrently lowering NBO:BO ratio. The proportion of  $\text{FAlCa}$  and  $\text{FAlCa}_2$  species both increased from G3 to G4 (increase of F content), agreeing with trends uncovered with  $^{27}\text{Al}$  and  $^{19}\text{F}$  MAS-NMR.<sup>68</sup> In Na-containing G338, 71% of fluorine binds Na (Table S12, ESI†), revealing the bases for the observed higher diffusion of  $\text{F}^-$  in G338. Fluoride is less strongly bound to  $\text{Na}^+$  due to its weaker charge field than that of  $\text{Ca}^{2+}$ . This arises from the two ions having near-identical ionic radii, yet  $\text{Ca}^{2+}$ , bearing double the charge. In fact, the strength of Na-F bond,<sup>79</sup> which is about  $10$  kcal mol<sup>-1</sup> lower than the Ca-F bond,<sup>79</sup> allows fluoride ions to more easily diffuse in glasses with higher  $\text{Na}^+:\text{Ca}^{2+}$  content. As a comparison, the diffusion rate of the oxygen atoms of water (mean residence time) in the first coordination shell of sodium ions (8 ps)<sup>80</sup> is one order of magnitude lower than that of  $\text{Ca}^{2+}$  (105 ps).<sup>81</sup>

Towards resolving the role of phosphate and sodium on fluorine diffusion, we computed the diffusion coefficients of fluorine ( $D_F$ ) (Table S13, ESI† and Fig. 7). Increases to the values of  $D_F$  of 15% and 25% were observed on going from G3 to G4 to G338 glasses, respectively ( $D_F \sim 0.261 \rightarrow 0.303 \rightarrow 0.365 \times 10^{-5}$  cm<sup>2</sup> s<sup>-1</sup>). A near linear relationship (adjusted  $R^2 = 0.9252$ ) is observed for  $\text{F}^-$  content's influence on  $D_F$ , with the absolute values comparable to the values computed for ions in



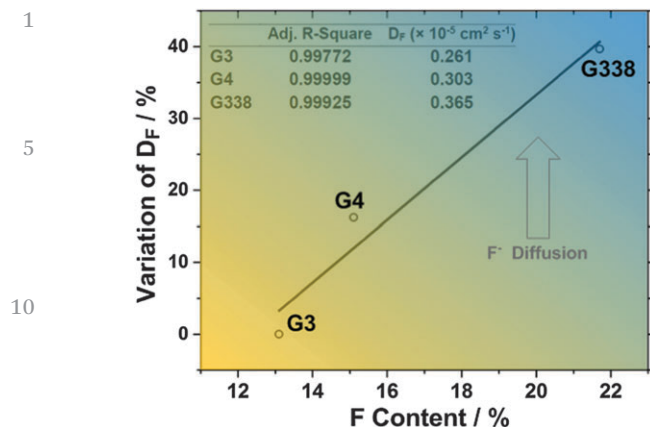


Fig. 7 Variation of fluorine self-diffusion coefficient ( $D_F$ ) with fluorine content in the G3, G4 and G338 ionomer glasses. The raised Na-content in G338 results in a predominance of F–Na binding (over F–Ca), affecting a significant increase in F-diffusion relative to the G3 and G4 glasses.

phosphosilicate glasses.<sup>57</sup> This represents an overall  $\sim 40\%$  increase in  $D_F$ , promoting clinically and practically favourable fluoride-release.<sup>7</sup>

With respect to Ca-coordination, Ca–O tends to higher coordination (8, 5, 6 CN of highest fraction for G3, G4, G338, respectively) than Ca–F (2, 1, 3), indicating preferential bonding between Ca–O over Ca–F. The three glasses also show Si–F bonding, whose first peaks of RDF all occur at 1.63 Å (Fig. S5, ESI<sup>†</sup>).

## Conclusions

We have reported the first ever-computational models of the glass component of bioactive glass ionomer cements. A full *ab initio* (density functional theory) melt-and-quit approach followed by 100 ps of molecular dynamics simulations at room temperature was used to generate the structure of three glasses relevant to bioactive ionomer cements, including commercial G338.

Based on the analysis of the short- and medium-range structures and associated dynamics of the glasses we conclude the following:

- Overall Al-coordination showed statistically significant increases with rising F content. Inter-atomic bonding in the three glasses showed atomic-pairs to be static, with the exceptions of Al–F, which was elongated and compressed, respectively, with increased F content.

- Three-center angular distribution functions were uniform across the three glasses with the exception of O–Al–F and O–Al–O, which showed considerable reduction in angular flexibility translating to an overall constraint at local aluminium pivots, as identified in THz and neutron experiments.<sup>40</sup> These hinge-points facilitate or impede compressions and expansions – giving rise to local structural flexibility and potentially damage tolerance. This indirectly agrees with established empirical determinations suggesting that over cross-linking results in Al-constraint and associated inflexibility.

- The addition of F and P (G4) and subsequently Na (G338) into the glass leads to a more marked oscillatory behavior of the VACF and a shift towards lower times. This is indicative of strengthening of Al-interaction with its neighboring atoms, and a more rigid intra-tetrahedral vibration, and further highlights the local constraint of Al to a definite and inflexible geometry.

- Increase of phosphorus content induced experimentally observed alumino-phosphate speciation of the bulk. The Al–P radial distribution functions showed speciation occurring below the clustering point, increasing with F-content.

- F–Na bonding and a concurrent reduction in F–Ca bonding occurred with increased F-content. The dominance of the weaker F–Na linkages resulted in a  $\sim 40\%$  increase in the fluorine diffusion coefficients.

The trends uncovered in the short- and medium-range structural parameters, as well as in the dynamical properties of the ionomer glasses considered in the present work suggest an overall atomistic-level stiffening/rigidifying of the glasses with rising P, F and Na content, and an overall predisposition of the practically relevant G338 glass to inflexibility. This atomistic detailing of the role of each atomic contributor to the bulk glass component could be instrumental in the formulation of a series of design rules in the rational optimisation of bioactive cements, while perhaps informing other cementitious material systems.

## Acknowledgements

K. V. T. thanks ETT-489/2009 and TAMOP-4.2.1.B, Hungary. D. D. T. thanks the UK's Royal Society for the award of a Royal Society Industry Fellowship. This research utilised Queen Mary's MidPlus computational facilities, supported by QMUL Research-IT and funded by EPSRC grant EP/K000128/1. *Via* our membership of the UK's HEC Materials Chemistry Consortium, which is funded by EPSRC (EP/L000202), this work used the ARCHER UK National Supercomputing Service (<http://www.archer.ac.uk>).

## Notes and references

- 1 P. D. Constantino and C. D. Freidman, *Otolaryngol. Clin. North Am.*, 1994, **27**, 1037–1073.
- 2 J. W. Nicholson, *Biomaterials*, 1998, **19**, 485–494.
- 3 A. D. Wilson and B. E. Kent, *J. Appl. Chem. Biotechnol.*, 1971, **21**, 313.
- 4 A. D. Wilson and B. E. Kent, *Br. Dent. J.*, 1972, **15**, 133–135.
- 5 BIO Intelligence Service, 2012, Study on the potential for reducing mercury pollution from dental amalgam and batteries, Final report prepared for the European Commission – DG ENV.
- 6 U. Ripamonti, L. C. Roden and L. F. Renton, *Biomaterials*, 2012, **33**, 3813–3823.
- 7 WHO, Atraumatic Restorative Treatment – A new approach for controlling dental caries, <http://toxicteeth.org/CAPP-ART.pdf>.

- 1 8 M. Dorri, A. Sheiham and V. C. C. Marinho, 2009, ART *versus* conventional restorative treatment for the management of dental caries. (Protocol).
- 9 Y. Takahashia, S. Imazatoa, A. V. Kaneshiroa, S. Ebisua, J. E. Frenckenb and F. R. Tayc, *Dent. Mater.*, 2006, **19**, 647–652.
- 10 A. W. G. Walls, *J. Dent.*, 1986, **14**, 231–246.
- 11 J. W. Nicholson and B. Czarnecka, *J. Biomater. Appl.*, 2009, **24**, 293–308.
- 12 L. Forsten and Scand, *J. Dent. Res.*, 1977, **85**, 503–504.
- 13 A. D. Wilson, D. M. Groffman and A. T. Kuhn, *Biomaterials*, 1985, **6**, 431–433.
- 14 B. F. El Mallakh and N. K. Sarkar, *Dent. Mater.*, 1990, **6**, 118–122.
- 15 15 M. L. Swartz, R. W. Phillips and H. E. Clark, *J. Dent. Res.*, 1984, **63**, 158–160.
- 16 R. G. Craig, *Restorative dental materials*, Mosby-Year Book, Inc., St Louis, MO, 10th edn, 1997.
- 17 P. Hotz, J. W. McLean, I. Sced and A. D. Wilson, *Br. Dent. J.*, 1977, **142**, 41–47.
- 18 H. Ngo, G. J. Mount and M. C. Peters, *Quint. Int.*, 1997, **28**, 63–69.
- 19 H. E. Sennou, A. A. Lebugle and G. L. Grégoire, *Dent. Mater.*, 1999, **15**, 229–237.
- 20 20 G. Geyer and J. Helms, *Eur. Arch. Otorhinolaryngol.*, 1993, **250**, 253–256.
- 21 J. W. Nicholson, *Proc. Inst. Mech. Eng., Part H*, 1998, **212**, 121–126.
- 22 W. R. Moore, S. E. Graves and G. I. Bain, *Aust. N. Z. J. Surg.*, 2001, **71**, 354–361.
- 23 P. V. Hatton, K. Hurrell-Gillingham and I. M. Brook, *J. Dent.*, 2006, **34**, 598–601.
- 24 L. M. Jonck, C. J. Grobbelaar and H. Strating, *Clin. Mater.*, 1989, **4**, 201–224.
- 25 25 L. M. Jonck and C. J. Grobbelaar, *Clin. Mater.*, 1990, **6**, 323–359.
- 26 E. Reusche, P. Pilz, G. Oberascher, B. Lindner, R. Egensperger, K. Gloeckner, E. Trinkka and B. Iglseider, *Hum. Pathol.*, 2001, **32**, 1136–1140.
- 27 27 I. M. Brook and P. V. Hatton, *Biomaterials*, 1998, **19**, 565–571.
- 28 S. Goldman, *J. Biomed. Mater. Res.*, 1985, **19**, 771–783.
- 29 A. Moshaverinia, N. Roohpour, W. W. L. Chee and S. R. Schricker, *J. Mater. Chem.*, 2011, **21**, 1319–1328.
- 30 30 A. Moshaverinia, N. Roohpour and W. W. L. Chee, *J. Mater. Chem.*, 2012, **22**, 2824–2833.
- 31 N. Zainuddin, N. Karpukhina, R. G. Hill and R. V. Law, *Dent. Mater.*, 2009, **25**, 290–295.
- 32 B. M. Culburtson, *Prog. Polym. Sci.*, 2001, **26**, 577–604.
- 33 33 L. L. Hench, R. J. Splinter, W. C. Alen and T. K. Greenlee, *J. Biomed. Mater. Res.*, 1971, **2**, 117–141.
- 34 A. D. Wilson, S. Crisp, H. J. Prosser, B. G. Lewis and S. A. Merson, *Ind. Eng. Chem. Prod. Res. Dev.*, 1980, **19**, 263–270.
- 35 35 B. E. Kent, B. G. Lewis and A. D. Wilson, *J. Dent. Res.*, 1979, **58**, 1607–1619.
- 36 S. G. Griffin and R. G. Hill, *Biomaterials*, 1999, **20**, 1579–1586.
- 37 S. G. Griffin and R. G. Hill, *Biomaterials*, 2000, **21**, 399–403.
- 38 S. G. Griffin and R. G. Hill, *J. Mater. Sci.*, 1998, **33**, 5383–5396.
- 39 A. D. Wilson, R. G. Hill, C. P. Warrens and B. G. Lewis, *J. Dent. Res.*, 1989, **68**, 89–94.
- 40 K. V. Tian, B. Yang, Y-Z. Yu, D. T. Bowron, J. Mayers, R. S. Donnan, C. Dobó-Nagy, J. W. Nicholson, D-C. Fang, A. L. Greer, G. A. Chass and G. N. Greaves, *Nat. Commun.*, 2015, DOI: 10.1038/ncomms9631.
- 41 J. Gaviria, C. G. García, E. Vélez and J. Quijano, *Model. Numer. Simul. Mater. Sci.*, 2013, **3**, 149–154.
- 42 J. VandeVondele, M. Krack, F. Mohamed, M. Parrinello, T. Chassaing and J. Hutter, *Comput. Phys. Commun.*, 2005, **167**, 103–128.
- 43 J. Hutter, M. Iannuzzi, F. Schiffmann and J. VandeVondele, *Wiley Interdiscip. Rev.: Comput. Mol. Sci.*, 2010, **4**, 15–25.
- 44 M. Dominik and J. Hutter, Ab initio molecular dynamics: Theory and Implementation, in *Modern Methods and Algorithms of Quantum Chemistry*, ed. J. Grotendorst, John von Neumann Institute for Computing, NIC Series 1. Julich, 2000, pp. 301–449.
- 45 A. Tilocca, *Proc. R. Soc. A*, 2009, **465**, 1003–1027.
- 46 A. Tilocca, *Phys. Chem. Chem. Phys.*, 2014, **16**, 3874–3880.
- 47 G. Lippert, J. Hutter and M. Parrinello, *Mol. Phys.*, 1997, **92**, 477–487.
- 48 J. P. Perdew, K. Burke and M. Ernzerhof, *Phys. Rev. Lett.*, 1996, **77**, 3865–3868.
- 49 J. K. Christie, R. I. Ainsworth and N. H. de Leeuw, *Biomaterials*, 2014, **35**, 6164–6171.
- 50 A. Tilocca and A. N. Cormack, *J. Phys. Chem. C*, 2008, **112**, 11936–11945.
- 51 J. K. Christie and A. Tilocca, *Adv. Eng. Mater.*, 2010, **12**, B326–B330.
- 52 S. Goedecker, M. Teter and J. Hutter, *Phys. Rev. B: Condens. Matter Mater. Phys.*, 1996, **54**, 1703–1710.
- 53 M. L. Öveçoğlu, B. Tarçun, H. S. Öveçoğlu, H. Gokce, G. Sinnmazisik and D. Turkyaydin, *Proceedings from the 5th International Congress on Adhesive Dentistry*, EGIS Publications, Philadelphia, Pennsylvania, Compend. Contin. Educ. Dent., June 14–15, 2013, vol. 34, p. 42.
- 54 A. Tilocca, *J. Chem. Phys.*, 2013, **139**, 114501.
- 55 55 D. Di Tommaso, R. I. Ainsworth, E. Tang and N. H. de Leeuw, *J. Mater. Chem. B*, 2013, **1**, 5054–5066.
- 56 E. Tang, D. Di Tommaso and N. H. de Leeuw, *Adv. Eng. Mater.*, 2010, **12**, B331–B338.
- 57 A. Tilocca, *Phys. Rev. B: Condens. Matter Mater. Phys.*, 2007, **76**, 224202.
- 58 J. K. Christie, A. Pedone, M. C. Menziani and A. Tilocca, *J. Phys. Chem. B*, 2011, **115**, 2038–2045.
- 59 P. Ganster, M. Benoit, J.-M. Delaye and W. Kob, *Mol. Simul.*, 2007, **33**, 1093–1103.
- 60 J. Schmidt, J. VandeVondele, I.-F. William Kuo, D. Sebastiani, J. Ilja Siepmann, J. Hutter and C. Mundy, *J. Phys. Chem. B*, 2009, **113**, 11959–11964.

- 1 61 Z. Strnad, *Biomaterials*, 1992, **13**, 317–321.
- 62 P. Lamparter and R. Knierp, *Physica B*, 1997, **234–236**, 405–406.
- 63 G. Gutiérrez and B. Johansson, *Phys. Rev. B: Condens. Matter Mater. Phys.*, 2002, **65**, 104202.
- 5 64 E. A. Chagarov and A. C. Kummel, *J. Chem. Phys.*, 2009, **130**, 124717.
- 65 A. Stamboulis, R. G. Hill and R. V. Law, *J. Non-Cryst. Solids*, 2004, **333**, 101–107.
- 10 66 A. Stamboulis, R. V. Law and R. G. Hill, *Biomaterials*, 2004, **25**, 3907–3913.
- 67 W. Lowenstein, *Am. Mineral.*, 1954, **39**, 92–94.
- 68 R. G. Hill, A. Stamboulis and R. V. Law, *J. Dent.*, 2006, **34**, 525–532.
- 15 69 R. G. Hill, A. D. Wilson and C. P. Warrens, *J. Mater. Sci.*, 1989, **24**, 363–371.
- 70 R. O. Ritchie, *Nat. Mater.*, 2011, **10**, 817–822.
- 71 M. T. Pedersen, K. V. Tian, C. Dobó-Nagy, G. A. Chass, G. N. Greavese and Y. Yue, *J. Non-Cryst. Solids*, 2015, **415**, 24–29.
- 20
- 25
- 30
- 35
- 40
- 45
- 50
- 55
- 72 J. P. Boon and S. Yip, *Molecular Hydrodynamics*, McGraw-Hill International Book Co., New York, 1980.
- 73 P. Demontis, G. B. Suffritti and A. Tilocca, *J. Chem. Phys.*, 1996, **105**, 5586.
- 74 E. A. Wasson and J. W. Nicholson, *Clin. Mater.*, 1991, **7**, 289–293. 5
- 75 E. A. Wasson and J. W. Nicholson, *J. Dent. Res.*, 1993, **7**, 481–483.
- 76 R. J. Kirkpatrick and R. K. Brow, *Solid State Nucl. Magn. Reson.*, 1995, **5**, 9–21. 10
- 77 R. Dupree, D. Holland, M. G. Mortuza, J. A. Collins and M. W. G. Lockyer, *J. Non-Cryst. Solids*, 1989, **112**, 111–119.
- 78 A. D. Wilson, *J. Mater. Sci. Lett.*, 1996, **15**, 275–276. **Q9**
- 79 *CRC Handbook of Chemistry and Physics*, ed. R. C. Weast, CRC Press, Boca Raton, FL, 55th edn, 1974. 15
- 80 D. Di Tommaso, E. Ruiz-Agudo, N. H. de Leeuw, A. Putnis and A. Putnis, *Phys. Chem. Chem. Phys.*, 2014, **16**, 7772–7785.
- 81 P. Raiteri, J. D. Gale, D. Quigley and P. M. Rodger, *J. Phys. Chem. C*, 2010, **114**, 5997–6010. 20
- 25
- 30
- 35
- 40
- 45
- 50
- 55